

# Electromigration-Induced Step Meandering on Vicinal Surfaces: Nonlinear Evolution Equation

Matthieu Dufay and Jean-Marc Debierre

*Laboratoire Matériaux et Microélectronique de Provence,  
Aix-Marseille Université and CNRS,  
Faculté des Sciences et Techniques de Saint-Jérôme,  
Case 151, 13397 Marseille Cedex 20, FRANCE*

Thomas Frisch

*Institut de Recherche sur les Phénomènes Hors Equilibre,  
Aix-Marseille Université, Ecole Centrale Marseille, and CNRS,  
49, rue Joliot Curie, BP 146, 13384 Marseille Cedex 13, FRANCE*

## Abstract

We study the effect of a constant electrical field applied on vicinal surfaces such as the Si(111) surface. An electrical field parallel to the steps induces a meandering instability with a nonzero phase shift. Using the Burton-Cabrera-Frank model, we extend the linear stability analysis performed by Liu, Weeks and Kandel (Phys. Rev. Lett. **81**, p.2743, 1998) to the nonlinear regime for which the meandering amplitude is large. We derive an amplitude equation for the step dynamics using a highly nonlinear expansion method. We investigate numerically two limiting regimes (small and large attachment lengths) which both reveal long-time coarsening dynamics.

PACS numbers: 66.30.Qa, 47.20.Hw

## I. INTRODUCTION

Stepped crystal surfaces exhibit a number of different morphological instabilities likely to play an important role during crystal growth<sup>1,2,3,4,5,6</sup>. Furthermore, the ability to control the growth of faceted stepped crystal surfaces may be of considerable importance when manufacturing electronic and optoelectronic devices<sup>7</sup>. These morphological instabilities occur not only during growth and evaporation but also under the influence of an electrical field, as on the well-studied Si(111) surface of a semiconductor. Surface electromigration instabilities may also arise in metals, where they are an important source of failure in microelectronic devices at metal-metal interfaces and also an interesting tool for pattern formation<sup>8,9</sup>. One of the most studied instability, known as step bunching, arises on the Si(111) surfaces from the biased diffusion (drift) of adatoms under the influence of an external driving force such as an electrical constant field<sup>10,11,12,13,14</sup>. Step bunching is a one-dimensional instability which has been explained within the framework of the Burton-Cabrera Frank equations<sup>15</sup> in terms of displacements of steps and terraces. Recent experimental and theoretical studies of step bunching revealed several difficulties, like the complex role of step transparency, the Ehrlich-Schwoebel barriers, the effect of substrate temperature, and the variations of the adatom mobility with the distance to the steps<sup>16,17,18,19</sup>.

In the present study, a constant electrical field is applied along the mean step direction of a train of synchronized steps (all identical up to a constant phase-shift). An experimental study of a comparable system was recently reported<sup>20</sup> and it was shown in this work that a two-dimensional step meandering instability takes place. The linear analysis of this problem was previously performed by Liu and co-authors who predicted the occurrence of synchronized meandering<sup>21</sup>. We perform here a nonlinear analysis of this instability in order to describe the long time behavior of the in-phase meandering mode. In particular we show the appearance of the coarsening regime in which steps undulations increase. This paper is organized as follows. In the next section, we present a model based on the Burton-Cabrera-Frank equations<sup>15</sup>. In the third section, we perform the linear analysis, which serves as a basis for the nonlinear analysis. A general nonlinear evolution equation including the effects of the repulsive step-step interactions is derived in section IV. The results of numerical simulations of this nonlinear equation are presented and discussed in section V, while conclusions and perspectives are postponed to section VI.

Before presenting our model, we shortly review previous work concerning nonlinear equations for the time evolution of synchronized steps. The step meandering instability was originally predicted theoretically by Bales and Zangwill<sup>22</sup> for a vicinal surface under growth. Its origin is the asymmetry between the descending and ascending currents of adatoms. As shown by Bales and Zangwill, a straight train of step may become morphologically unstable during MBE growth if the kinetic attachment at the steps is asymmetrical: this is the Ehrlich-Schwoebel effect. It was shown that the most dangerous mode corresponds to a zero phase-shift<sup>23</sup>. Nonlinear extensions of this work have shown that the meander evolution can be described by amplitude equations displaying diverse behaviors. Close to the instability threshold, starting from the Burton-Cabrera-Frank (BCF) model, it was proved<sup>24</sup> that the step position in the presence of desorption (evaporation) obeys the Kuramoto-Sivashinsky equation. The ultimate stage of this dynamics is thus spatio-temporal chaos. In the case of negligible desorption with strong or moderate Ehrlich-Schwoebel effect, it was found that the step amplitude obeys a highly nonlinear equation.<sup>25,26,27</sup> This equation cannot be derived from a weakly nonlinear analysis but is based on the assumption that the slope of the steps is of order unity. Instead of spatio-temporal chaos, a regular pattern is revealed: the lateral modulation wavelength is fixed while the transverse amplitude of the step deformation (meandering amplitude) increases. Elasticity or diffusion anisotropy can also influence the meander dynamics.<sup>28,29</sup> It was recently shown in context of the step meandering instabilities during growth on Si(001)<sup>30,31</sup> that the nonlinear dynamics is driven by a conserved Kuramoto-Sivashinsky equation. This equation was already mentioned in Ref.<sup>27</sup> on the basis of symmetry arguments but was not derived there, because of a different scaling of the Ehrlich-Schwoebel effect. Step meandering was also studied in the context of electromigration<sup>32,33,34</sup> using analytic linear analysis and kinetic Monte Carlo simulations. It is therefore of importance to extend the work of Liu *et al*<sup>21</sup> and to develop analytical tools to describe the nonlinear regime of the meandering instability.

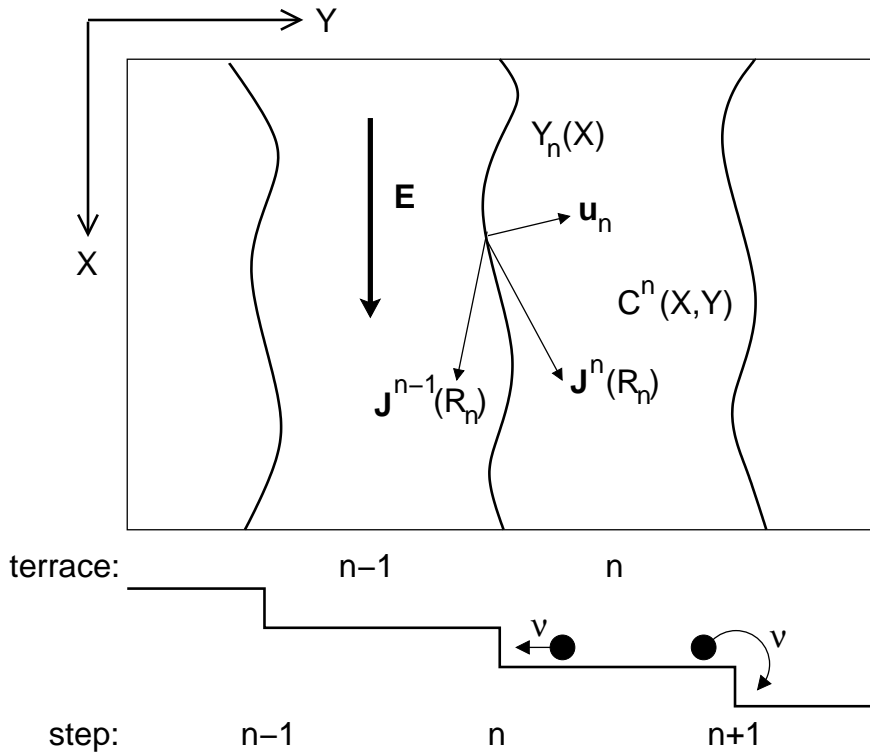


FIG. 1: Schematic representation of a small portion of a vicinal surface showing three steps. On the top view (above), the electrical field  $\mathbf{E}$  is represented. On the side view (below), two attachment mechanisms are illustrated.

## II. MODEL

### A. Validity range and notations

The geometry of the problem is sketched in Fig. (1). Initially, all the step edges are directed along the  $X$  axis, and equidistant from a distance  $L_0$ . A constant electrical field  $E$  is applied in the positive  $X$  direction. To investigate the resulting meandering instability, we use a two-dimensional version of the BCF model. The terraces are numbered sequentially in the step-down direction. In our notations, the  $n$ -th terrace is bordered by the two steps numbered  $n$  and  $n + 1$ . To distinguish between quantities defined anywhere on the terrace and quantities defined at steps only, we will use an upper index  $n$  in the first case and a lower index  $n$  in the second. For instance, the adatom concentration on the  $n$ -th terrace is denoted  $C^n$ , while the equilibrium concentration at step  $n$  reads  $C_n^{eq}$ .

In practice, it is usually assumed that the concentrations are not explicitly time-

dependent, so that  $C^n = C^n(X, Y)$ . This quasi-static approximation is valid provided that the diffusion coefficient  $D_s$  of the adatoms on the terraces is sufficiently large that diffusion takes place on time scales shorter than those for step motion. The diffusion bias introduced by the electrical field can be quantified by the ratio of the thermal energy  $k_B T$  to the electrical energy  $|Z^* e| E \ell_E$ . Balancing the two terms defines the electrical length as

$$\ell_E = \frac{k_B T}{|Z^* e| E}, \quad (1)$$

where  $k_B$  is the Boltzmann constant,  $T$  the absolute temperature,  $Z^*$  the effective atomic charge number, and  $e$  the electron electrical charge.

For the sake of simplicity, we set both deposition and evaporation of adatoms to zero here, whereas experiments are usually performed with a small but nonzero net flux. Introducing both effects in our model is straightforward and would not affect qualitatively the results obtained within the zero flux assumption.

On the  $n$ -th terrace, the quasi-static biased diffusion equation reduces to

$$D_s(\partial_{XX} + \partial_{YY})C^n - (D_s/\ell_E)\partial_X C^n = 0, \quad (2)$$

and the adatom flux is

$$\mathbf{J}^n = D_s(1/\ell_E - \partial_X, -\partial_Y)C^n. \quad (3)$$

The boundary conditions for Eq. (2) are obtained by writing mass conservation at all the points  $\mathbf{R}_n = (X, Y_n)$  and  $\mathbf{R}_{n+1} = (X, Y_{n+1})$  located on both edges of the terrace. In the present model, we assume that the adatom attachment/detachment kinetic coefficients are the same on the upper and lower side of a given step,  $\nu^+ = \nu^- = \nu$ . We further restrict ourselves to temperature ranges where direct mass exchange between adjacent terraces (transparency) can be neglected. At  $\mathbf{R}_n$ , the boundary condition thus reads

$$\mathbf{J}^n(\mathbf{R}_n) \cdot \mathbf{u}_n = -\nu[C^n(\mathbf{R}_n) - C_n^{eq}], \quad (4)$$

where  $\mathbf{u}_n$  represents the normal unit vector pointing in the step-down direction. Alternatively, at  $\mathbf{R}_{n+1}$ , the second boundary condition is

$$\mathbf{J}^n(\mathbf{R}_{n+1}) \cdot \mathbf{u}_{n+1} = \nu[C^n(\mathbf{R}_{n+1}) - C_{n+1}^{eq}]. \quad (5)$$

Writing mass conservation at any point  $\mathbf{R}_n$  along step  $n$ , we obtain the normal (component along  $\mathbf{u}_n$ ) step velocity,

$$V_n = \Omega_s \nu [C^n(\mathbf{R}_n) + C^{n-1}(\mathbf{R}_n) - 2C_n^{eq}]. \quad (6)$$

In this equation,  $\Omega_s$  is the adatom area and we neglect adatom diffusion along the step.

## B. Nondimensional version of the governing equations

The terrace width  $L_0$  provides a natural length scale for the problem. Another possibility is the electrical length  $\ell_E$  defined in Eq. (1). However, since  $\ell_E$  is likely to diverge as the electrical field goes to zero,  $L_0$  is preferred. Setting

$$x = \frac{X}{L_0}, \quad y = \frac{Y}{L_0}, \quad \frac{1}{\eta} = \frac{\ell_E}{L_0}, \quad c^n = \frac{C^n}{C_0}, \quad (7)$$

where  $C_0\Omega_s$  is the fraction of adsorption sites occupied by adatoms, we get the nondimensional form of Eqs. (2-6). The quasistatic diffusion equation reads

$$(\partial_{xx} + \partial_{yy} - \eta\partial_x)c^n = 0, \quad (8)$$

and the adatom flux is

$$\mathbf{j}^n = (\eta - \partial_x, -\partial_y)c^n. \quad (9)$$

In this equation, the nondimensional flux vector is defined as

$$\mathbf{j}^n = \frac{L_0}{D_s C_0} \mathbf{J}^n, \quad (10)$$

so that the physical time is rescaled by the characteristic time

$$t_0 = \frac{1}{D_s C_0}. \quad (11)$$

Using both the time and space scale factors, we obtain the first,

$$\mathbf{j}^n(\mathbf{r}_n) \cdot \mathbf{u}_n = -\rho[c^n(\mathbf{r}_n) - c_n^{eq}], \quad (12)$$

and the second boundary condition,

$$\mathbf{j}^n(\mathbf{r}_{n+1}) \cdot \mathbf{u}_{n+1} = \rho[c^n(\mathbf{r}_{n+1}) - c_{n+1}^{eq}]. \quad (13)$$

The nondimensional number,

$$\rho = \frac{\nu L_0}{D_s}, \quad (14)$$

inversely proportional to the characteristic length  $d = D_s/\nu$ , indicates which mechanism between diffusion and attachment governs the time evolution of the steps. The normal velocity of step  $n$  now takes the form,

$$v_n = \sigma\rho[c^n(\mathbf{r}_n) + c^{n-1}(\mathbf{r}_n) - 2c_n^{eq}], \quad (15)$$

where

$$\sigma = \frac{\Omega_s}{L_0^2} \quad (16)$$

is the ratio of the two basic areas in the problem.

### C. Equilibrium concentration

We now derive a detailed expression of the equilibrium concentration  $c_n^{eq}$  at step  $n$ . A quite general form is

$$c_n^{eq} = C_n^{eq}/C_0 = \exp\left(\frac{M}{k_B T}\right) = 1 + \frac{M}{k_B T} + \dots \quad (17)$$

We will use the thermal energy  $k_B T$  as the energy scale, and define the nondimensional chemical potential as

$$\mu = \frac{M}{k_B T}. \quad (18)$$

Within the nondimensional description presented in previous section, the position of step  $n$  is represented by a function  $y_n(x)$ , and we define the relative position as

$$\zeta_n(x) = y_n(x) - n. \quad (19)$$

Following Paulin and coworkers,<sup>28</sup> we introduce a nondimensional free energy functional for step  $n$ ,

$$f_n = f_n^R + f_n^I. \quad (20)$$

The first term is due to the step stiffness,

$$f_n^R = \beta \int_n ds. \quad (21)$$

Here  $\int_n ds$  is the integral of the curvilinear abscissa along the whole step  $n$  (total step length) and  $\beta = B(L_0/k_B T)$ , where  $B$  is the step-stiffness of the material. The second term sums up the step-step repulsive energies assumed to vary as the inverse square distance,

$$f_n^I = \frac{\alpha}{2} \int_n \left[ \left(\frac{1}{l_n^+}\right)^2 + \left(\frac{1}{l_n^-}\right)^2 \right] ds, \quad (22)$$

where  $\alpha = A/(k_B T L_0)$ , and  $A$  is the step interaction coefficient. As shown in Fig. (2), the lengths  $l_n^+$  and  $l_n^-$  are the shortest distances between steps  $(n, n+1)$  and steps  $(n, n-1)$ .

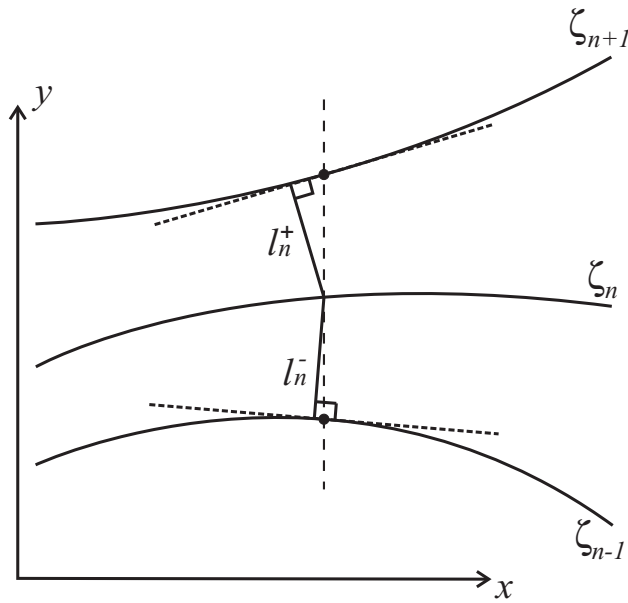


FIG. 2: Shortest distances between a given step and its two closest neighbors, in the general case. The tangents to steps  $n - 1$  and  $n + 1$  are drawn at two points having the same abscissa  $x$ .

Thus the previous relation gives only an approximate value of the total repulsion energy. Finally, the chemical potential is obtained by a functional derivation of the free energy,

$$\mu = \sigma \left( \frac{\delta f_n}{\delta \zeta_n} \right). \quad (23)$$

### III. LINEAR STABILITY ANALYSIS

Repulsions between steps prevent them from intersecting one-another and edge stiffness limits their curvature. However, the possibility that the shapes of two consecutive steps are weakly correlated in phase or amplitude remains open. Since the general problem is quite difficult to solve in practice, we limit the present study to the simple case of a synchronized train of steps.

Starting with straight steps, separated by a unit distance, we introduce an harmonic perturbation of amplitude  $\epsilon \ll 1$ , wave number  $q$ , and phase-shift  $\phi$ ,

$$\zeta_n(x) = \epsilon \exp(iqx + \omega t + in\phi). \quad (24)$$



Looking for solutions of the nondimensional diffusion equation under the form

$$c^n(x, y) = 1 + c_1^n(y)\zeta_n(x), \quad (25)$$

we obtain

$$c_1^n(y) = A_1^n e^{ry} + B_1^n e^{-ry}, \quad (26)$$

with

$$r = \sqrt{q^2 + i\eta q}. \quad (27)$$

To derive the dispersion relation, we first express the chemical potential using Eqs. (20-23). In practice, the step curvature is small, and an accurate approximation of the step-step distances is given by

$$l_n^+ = \frac{1 + \zeta_{n+1} - \zeta_n}{\sqrt{1 + (\partial_x \zeta_{n+1})^2}} \quad \text{and} \quad l_n^- = \frac{1 + \zeta_n - \zeta_{n-1}}{\sqrt{1 + (\partial_x \zeta_{n-1})^2}} \quad (28)$$

To the leading order in the perturbation amplitude  $\epsilon$ , we find the chemical potential from Eqs. (20-24,28),

$$\mu = \sigma \zeta_n g(q, \phi), \quad (29)$$

where

$$g(q, \phi) = (\alpha + \beta) q^2 + 6\alpha(1 - \cos \phi). \quad (30)$$

Introducing this result in Eqs. (12,13,15), the following dispersion relation is finally obtained,

$$\frac{\omega(q, \phi)}{2\sigma r} = \frac{q_\rho^2 \sin \phi + \sigma(\cos \phi - \cosh r - \frac{r}{\rho} \sinh r)g(q, \phi)}{(1 + \frac{r^2}{\rho^2}) \sinh r + 2\frac{r}{\rho} \cosh r}. \quad (31)$$

This equation is similar to the dispersion relation derived in Ref.<sup>21</sup>. In the remaining of this section, we will neglect the step-step interactions,  $\alpha = 0$ , to avoid unnecessarily complicated relations. Keeping the actual value of  $\alpha$  would only introduce small quantitative changes. The growth rate is defined as  $\Gamma(q, \phi) = \text{Re}(\omega)$ . A meandering instability is thus expected for positive values of  $\Gamma$ . Experimentally, the electrical field is a weak perturbation, so that, according to Eq. (7), the parameter  $\eta$  takes small values ( $\simeq 10^{-8} - 10^{-4}$ ). We thus expect the wave numbers of the corresponding instabilities to verify  $q \ll 1$ . As we do not know *a priori* the relative magnitude of  $\eta$  and  $q$ , we first use a general expansion in which both

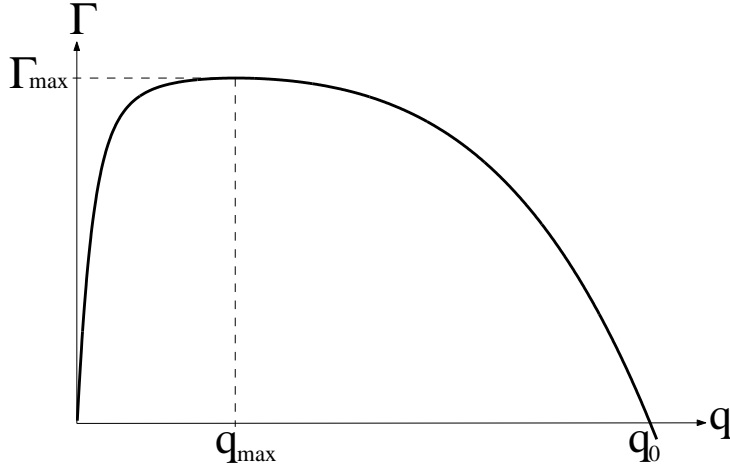


FIG. 3: Plot of the growth rate  $\Gamma(q, \phi^*) = \text{Re}(\omega)$  obtained from the linear stability analysis Eq. (31) as a function of the perturbation wave number  $q$ .

quantities are small and considered equivalently. This leads to

$$\begin{aligned}
\Gamma = & \frac{2}{2+\rho} \sigma \eta \sin \phi q - \frac{2\rho}{2+\rho} \sigma^2 \beta (1 - \cos \phi) q^2 \\
& - \frac{1}{3} \frac{\rho^2 + 6\rho + 6}{\rho(2+\rho)^2} \sigma \eta \sin \phi q^3 \\
& - \frac{1}{3} \frac{\rho^2 + (\rho^2 + 6\rho + 6)(1 + \cos \phi)}{(2+\rho)^2} \sigma^2 \beta q^4 \\
& + \dots
\end{aligned} \tag{32}$$

Although the two last terms are of higher order, we nevertheless keep them since the lowest order terms vanish when  $\phi = 0$ . A first necessary condition for a maximally unstable mode,  $(\partial\Gamma/\partial\phi)_q = 0$ , gives the following phase-shift:

$$\phi^*(q) = \tan^{-1} \left( \frac{\eta}{\sigma \rho \beta q} \right). \tag{33}$$

The corresponding growth rate,  $\Gamma(q, \phi^*)$ , is plotted as a function of the wave number  $q$  in Fig. (3): a meandering instability arises as soon as the electrical field is nonzero.<sup>21</sup> For  $q \gg \eta$ , it is possible to find relations between  $q$  and  $\eta$  in different ranges of wave numbers. The most unstable mode  $q = q_{max}$  is obtained by introducing the second condition  $(\partial\Gamma/\partial q)_\phi = 0$ . Together with Eq. (33), we get

$$q_{max} = \left( \frac{1}{2\rho} \right)^{\frac{1}{2}} \left( \frac{1}{2+\rho} \right)^{\frac{1}{6}} \left( \frac{\eta}{\sigma\beta} \right)^{\frac{2}{3}}, \tag{34}$$

and the absolute maximum of the amplification factor is

$$\Gamma_{max} = \Gamma(q_{max}, \phi^*) = \frac{\eta^2}{\beta\rho(2 + \rho)}. \quad (35)$$

Finally, the marginal mode  $q = q_0$  is deduced from the condition  $\Gamma(q, \phi^*) = 0$ :

$$q_0 = \left(\frac{1}{\rho}\right)^{\frac{1}{4}} \left(\frac{1}{2 + \rho}\right)^{\frac{1}{4}} \left(\frac{\eta}{\sigma\beta}\right)^{\frac{1}{2}}. \quad (36)$$

The scalings of  $q_{max}$  and  $q_0$  with  $\eta$  thus suggest that the range of unstable modes is quite large. The limit of weak electrical fields ( $\eta \ll 1$ ) is relevant for the experimental work reported in Ref.<sup>20</sup>, in which step meandering is observed. In addition, the maximum growth rate being small, the situation is favorable for a nonlinear analysis of the meandering instability which is presented in the next section.

## IV. NONLINEAR ANALYSIS

### A. Local coordinates

As illustrated in Fig. (4), we consider the case of steps which are all identical up to a translation in an oblique direction  $\tilde{z}$  rotated by an angle  $\theta$  with respect to axis  $y$ . The amplitudes of two successive steps have thus the following property:

$$\zeta_{n+1}(x - \tan \theta) = \zeta_n(x). \quad (37)$$

In the linear regime defined by Eq. (24), we have

$$\theta \simeq \tan^{-1}(\phi/q). \quad (38)$$

Since we want to explore nonlinear dynamics, the amplitude of the meanders may reach values of order unity for which  $\zeta_n(x)$  is no more a single-valued function in the original frame of reference  $(x, y)$ . For this reason, our nonlinear model makes use of a non-orthogonal frame of reference  $(\tilde{x}, \tilde{z})$ , defined as

$$\begin{aligned} \tilde{x} &= x + y \tan \theta, \\ \tilde{z} &= \frac{y}{\cos \theta}, \end{aligned} \quad (39)$$

as shown in Fig. (4). With this change of coordinates, the step shape function becomes

$$\xi(\tilde{x}) = \frac{\zeta_n(x - n \tan \theta)}{\cos \theta}, \quad (40)$$

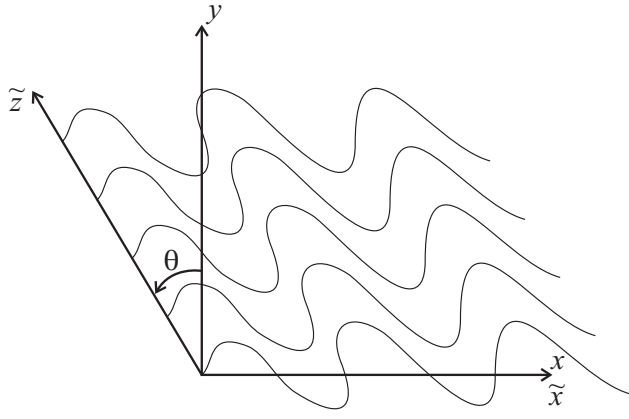


FIG. 4: A set of steps identical up to a translation along the  $\tilde{z}$  axis. The local variables used in the nonlinear analysis are  $\tilde{z} = y/(\cos \theta)$  and  $\tilde{x} = x + y \tan \theta$ .

where the  $n$  index can be omitted because all the steps are identical in the new frame. We further define a local frame of reference  $(\chi, \psi)$  by moving the  $\tilde{x}$  and  $\tilde{z}$  axes along the step,

$$\begin{aligned}\chi &= \tilde{x}, \\ \psi &= \tilde{z} - \xi(\tilde{x}) = \tilde{z} - \xi(\chi).\end{aligned}\tag{41}$$

In the local frame, the partial derivatives transform as

$$\begin{aligned}\partial_x &= \partial_\chi - (\partial_\chi \xi) \partial_\psi, \\ \partial_y &= \tan \theta \partial_\chi + \left( \frac{1}{\cos \theta} - \tan \theta \partial_\chi \xi \right) \partial_\psi,\end{aligned}\tag{42}$$

where  $\partial_\chi \xi = \partial \xi / \partial \chi$ . The second derivatives are derived from these expressions.

### B. BCF equations for the local coordinates

Introducing the relations for the partial derivatives into Eq. (8), one gets the quasi-static diffusion equation for the local coordinates  $(\chi, \psi)$ ,

$$\begin{aligned}0 &= [\partial_{\chi\chi} + p^2 \partial_{\psi\psi} + (\eta \cos^2 \theta \partial_\chi \xi - \partial_{\chi\chi} \xi) \partial_\psi \\ &\quad + 2(\sin \theta - \partial_\chi \xi) \partial_{\chi\psi} - \eta \cos^2 \theta \partial_\chi] c(\chi, \psi),\end{aligned}\tag{43}$$

where

$$p(\chi) = \sqrt{(1 - \sin \theta \partial_\chi \xi)^2 + (\cos \theta \partial_\chi \xi)^2}.\tag{44}$$

Note that the step index  $n$  is purposely omitted because of translational invariance. It is easier to express the vectorial quantities in the base of the two unit vectors of the initial frame  $(x, y)$ . The adatom flux reads

$$\begin{aligned} \mathbf{j} = (j_x, j_y) = c(\chi, \psi) & \left( -\partial_\chi + (\partial_\chi \xi) \partial_\psi + \eta, \right. \\ & \left. - \tan \theta \partial_\chi - \frac{1}{\cos \theta} \partial_\psi + (\partial_\chi \xi) \tan \theta \partial_\psi \right), \end{aligned} \quad (45)$$

and the unit normal vector to the step,

$$\mathbf{u} = \frac{1}{p} \left( -\cos \theta \partial_\chi \xi, 1 - \sin \theta \partial_\chi \xi \right). \quad (46)$$

The two boundary conditions take on very simple forms,

$$\begin{aligned} \mathbf{j} \cdot \mathbf{u} &= -\rho(c - c^{eq}) \quad \text{at} \quad \psi = 0, \\ \mathbf{j} \cdot \mathbf{u} &= +\rho(c - c^{eq}) \quad \text{at} \quad \psi = \frac{1}{\cos \theta}. \end{aligned} \quad (47)$$

The expression of the local curvature is needed to complete these boundary conditions. We obtain

$$\kappa(\chi) = -\frac{\cos \theta}{p^3} \partial_{\chi\chi} \xi. \quad (48)$$

The normal velocity is deduced from Eq. (15),

$$v(\chi) = \frac{\partial_t \xi}{p} = \sigma \rho \left[ c(\chi, 0) + c\left(\chi, \frac{1}{\cos \theta}\right) - 2c^{eq}(\chi) \right], \quad (49)$$

where  $c^{eq}(\chi) \simeq 1 + \mu(\chi)$ . An expression for the chemical potential is obtained through the functional derivative of the free energy functional, Eqs. (20-23). In the oblique frame of reference, we have now,

$$\mu = \frac{\sigma}{\cos \theta} \left( \frac{\delta f}{\delta \xi} \right), \quad (50)$$

and the curvilinear length element is  $ds = p d\chi$ . As illustrated in Fig. (5) the shortest step-step distances are defined in a slightly different way in this frame: the tangents to the two adjacent steps are drawn at a given value of  $\tilde{x}$ . Adapting Eq. (28) to this new definition, we obtain

$$l^+ = \frac{\frac{1}{\cos \theta} + \xi_+ - \xi}{p_+} \quad \text{and} \quad l^- = \frac{\frac{1}{\cos \theta} + \xi - \xi_-}{p_-}, \quad (51)$$

where

$$p_\pm = \sqrt{(1 - \sin \theta \partial_\chi \xi_\pm)^2 + (\cos \theta \partial_\chi \xi_\pm)^2}. \quad (52)$$

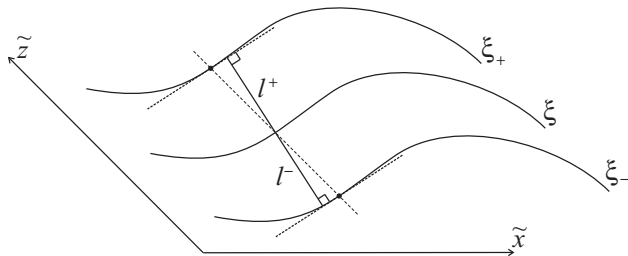


FIG. 5: Shortest distances between a given step and its two closest neighbors, in the local frame. The case of translational invariance along  $\tilde{z}$  is represented here. The tangents to the adjacent steps are drawn at two points having the same abscissa  $\tilde{x}$ .

Note that it is necessary to keep the amplitudes  $\xi_-$ ,  $\xi$ , and  $\xi_+$  of three successive steps to perform the functional derivation. After derivation, we set  $\xi = \xi_{\pm}$ , so that  $l_+ = l_- = l$ , and,

$$\mu(\chi) = \sigma\kappa \left\{ \beta + \frac{\alpha}{l^2 \cos^2 \theta} \left[ p^2 + (\partial_x \xi - \sin \theta)^2 \right] \right\}. \quad (53)$$

The chemical potential sums up the contributions of the step stiffness and of the step-step interactions.

### C. Small parameter expansion

The aim of this paragraph is to establish a nonlinear equation for the time evolution of a step.

#### 1. Scaled variables

In the linear analysis presented above, we have shown that the wave number  $q_0 \sim \eta^{1/2}$  is small as compared to unity in the limit of a weak electrical field. We thus introduce a small parameter  $\epsilon \ll 1$ , such as

$$\eta = \epsilon^2 \eta_2. \quad (54)$$

and  $\eta_2$  is of order unity. As a consequence, we define the slow space variable

$$x = \epsilon \chi. \quad (55)$$

Note that the slow  $x$  variable used hereafter differs from the fast  $x$  variable discussed in section II. This should not introduce any confusion, since only the new  $x$  appears in the

following. At the marginal wave number  $q = q_0$ , the linear analysis results of Eqs. (33, 36, 38) give the following relation between the inclination angle  $\theta$  and the non-dimensional number  $\rho$ ,

$$\theta \simeq \tan^{-1} \left( \left( \frac{2 + \rho}{\rho} \right)^{\frac{1}{2}} \right). \quad (56)$$

Since  $\rho$  can be large or small depending on the parameters,  $\theta$  can take arbitrary values. The boundary conditions given in Eq. (47) are applied at  $\psi = 0$  and  $\psi = 1/\cos\theta$ , so that the space variable  $\psi$  is simply equal to  $z$ . Accordingly, one defines the meander amplitude as  $h(x) = \xi(\chi)$  and the normal velocity as  $\tilde{v}(x) = v(\chi)$ .

## 2. Order by order expansion

The unknown variables, concentration and shape function are expressed as power expansions of the scaling parameter  $\epsilon$ ,

$$\begin{aligned} c(x, z) &= c_0(x, z) + \epsilon c_1(x, z) + \epsilon^2 c_2(x, z) + \dots \\ h(x) &= \epsilon^{-1} h_{-1}(x) + \epsilon^0 h_0(x) + \epsilon h_1(x) + \dots \\ \tilde{v}(x) &= \epsilon^3 \tilde{v}_3(x) \end{aligned} \quad (57)$$

Introducing this expression of  $h(x)$  in Eq. (44), the following development is found for  $p$ ,

$$p(x) = p_0(x) + \epsilon p_1(x) + \epsilon^2 p_2(x) + \dots, \quad (58)$$

with

$$p_0(x) = \sqrt{(1 - \sin\theta \partial_x h_{-1})^2 + (\cos\theta \partial_x h_{-1})^2}. \quad (59)$$

We obtain in a similar way the equilibrium concentration

$$c^{eq}(x) = 1 + \epsilon c_1^{eq}(x) + \epsilon^2 c_2^{eq}(x) + \dots, \quad (60)$$

where

$$c_1^{eq}(x) = -\sigma \cos\theta \frac{\partial_{xx} h_{-1}}{p_0^3} \left[ \beta + \alpha p_0^2 (2p_0^2 - \cos^2\theta) \right]. \quad (61)$$

We now solve order by order the nondimensional equations obtained by introducing the scaled variables defined above into Eqs.(43, 45, 47, 49). The results obtained at order  $i$  are used to derive the equations at order  $i + 1$ .

## order 0

The diffusion equation reduces to

$$p_0^2 \partial_{zz} c_0 = 0. \quad (62)$$

We look for solutions of the form

$$c_0(x, z) = a_0(x)z + b_0(x), \quad (63)$$

which imposes

$$\begin{aligned} p_0^2 a_0 - \rho p_0 \cos \theta [b_0 - 1] &= 0, \\ p_0^2 a_0 + \rho p_0 \cos \theta [b_0 - 1] + \rho p_0 a_0 &= 0, \end{aligned} \quad (64)$$

for the boundary conditions, so that,

$$\begin{aligned} a_0(x) &= 0, \\ b_0(x) &= 1, \\ c_0(x, z) &= 1. \end{aligned} \quad (65)$$

At this order, the velocity is found to be zero.

### order 1

Diffusion equation:

$$p_0^2 \partial_{zz} c_1 = 0. \quad (66)$$

Solution:

$$c_1(x, z) = a_1(x)z + b_1(x). \quad (67)$$

Boundary conditions:

$$\begin{aligned} p_0^2 a_1 - \rho p_0 \cos \theta [b_1 - c_1^{eq}] &= 0, \\ p_0^2 a_1 + \rho p_0 \cos \theta [b_1 - c_1^{eq}] + \rho p_0 a_1 &= 0. \end{aligned} \quad (68)$$

Solution:

$$\begin{aligned} a_1(x) &= 0, \\ b_1(x) &= c_1^{eq}(x), \\ c_1(x, z) &= c_1^{eq}(x). \end{aligned} \quad (69)$$

At this order, the velocity is found to be zero.



**order 2**

Diffusion equation:

$$p_0^2 \partial_{zz} c_2 = 0. \quad (70)$$

Solution:

$$c_2(x, z) = a_2(x)z + b_2(x). \quad (71)$$

Boundary conditions:

$$\begin{aligned} p_0^2 a_2 - \rho p_0 \cos \theta [b_2 - c_2^{eq}] + f_2 &= 0, \\ p_0^2 a_2 + \rho p_0 \cos \theta [b_2 - c_2^{eq}] + f_2 + \rho p_0 a_2 &= 0, \end{aligned} \quad (72)$$

with

$$f_2(x) = \eta_2 \cos^2 \theta \partial_x h_{-1} + (\sin \theta - \partial_x h_{-1}) \partial_x c_1^{eq}. \quad (73)$$

Concentration:

$$\begin{aligned} a_2(x) &= -\frac{2}{p_0(x)} \frac{f_2(x)}{2p_0(x) + \rho}, \\ b_2(x) &= c_2^{eq}(x) - \frac{a_2(x)}{2 \cos \theta}, \\ c_2(x, z) &= c_2^{eq}(x) + \left( z - \frac{1}{2 \cos \theta} \right) a_2(x). \end{aligned} \quad (74)$$

Zero normal velocity.

**order 3**

Diffusion equation:

$$p_0^2 \partial_{zz} c_3 - 2p_0^2 d_3 = 0. \quad (75)$$

with

$$d_3(x) = \frac{2(\partial_x h_{-1} - \sin \theta) \partial_x a_2 + a_2 \partial_{xx} h_{-1} - \partial_{xx} c_1^{eq}}{2 p_0^2}. \quad (76)$$

Solution:

$$c_3(x, z) = d_3(x)z^2 + a_3(x)z + b_3(x). \quad (77)$$

Boundary conditions:

$$\begin{aligned} p_0^2 a_3 - \rho p_0 \cos \theta [b_3 - c_3^{eq}] + f_3 &= 0, \\ p_0^2 a_3 + \rho p_0 \cos \theta [b_3 - c_3^{eq}] + f_3 + g_3 + \rho p_0 a_3 &= 0, \end{aligned} \quad (78)$$

with

$$\begin{aligned}
f_3(x) &= \frac{\partial_x h_{-1} - \sin \theta}{2 \cos \theta} \partial_x a_2 - \partial_x h_0 \partial_x c_1^{eq} \\
&+ \left[ 2 \left( \partial_x h_{-1} - \sin \theta \right) \partial_x h_0 - p_0 p_1 \right] a_2 \\
&+ \left[ \left( c_1^{eq} - \frac{p_1}{p_0} \right) \partial_x h_{-1} + \partial_x h_0 \right] \eta_2 \cos^2 \theta \\
&+ \left( \partial_x h_{-1} - \sin \theta \right) \left( \frac{p_1}{p_0} \partial_x c_1^{eq} - \partial_x c_2^{eq} \right), \tag{79}
\end{aligned}$$

and

$$g_3(x) = \frac{p_0(2p_0 + \rho)}{\cos \theta} d_3 - \frac{\partial_x h_{-1} - \sin \theta}{\cos \theta} \partial_x a_2. \tag{80}$$

Concentration:

$$\begin{aligned}
a_3(x) &= -\frac{1}{p_0} \frac{g_3 + 2f_3}{2p_0 + \rho} \\
b_3(x) &= c_3^{eq} + \frac{\rho f_3 - p_0 g_3}{\rho p_0 \cos \theta (2p_0 + \rho)} \\
c_3(x, z) &= d_3(x) z^2 + a_3(x) z + b_3(x) \tag{81}
\end{aligned}$$

The normal velocity is nonzero for the first time at this order. Its expression is derived by using Eq. (49) together with the scaling relations of section IV C 1,

$$\begin{aligned}
\tilde{v}_3(x) &= \frac{\sigma}{p_0 \cos^2 \theta} \partial_x \left[ \frac{2 \cos^2 \theta + \rho p_0}{p_0(\rho + 2p_0)} \partial_x c_1^{eq} \right. \\
&\left. - 2\eta_2 \cos^2 \theta \frac{\sin \theta - \partial_x h_{-1}}{p_0(\rho + 2p_0)} \partial_x h_{-1} \right]. \tag{82}
\end{aligned}$$

#### D. Amplitude equation

We finally obtain the following amplitude equation using Eqs. (49,82):

$$\begin{aligned}
\partial_t H &= \frac{\sigma}{\cos^2 \theta} \partial_x \left[ \frac{2 \cos^2 \theta + \rho p_0}{p_0(\rho + 2p_0)} \partial_x c_1^{eq} \right. \\
&\left. - 2\eta_2 \cos^2 \theta \frac{\sin \theta - \partial_x H}{p_0(\rho + 2p_0)} \partial_x H \right], \tag{83}
\end{aligned}$$

where

$$p_0(x) = \sqrt{(1 - \sin \theta \partial_x H)^2 + (\cos \theta \partial_x H)^2}, \tag{84}$$

and

$$c_1^{eq}(x) = -\sigma \cos \theta \frac{\partial_{xx} H}{p_0^3} \left[ \beta + \alpha p_0^2 (2p_0^2 - \cos^2 \theta) \right]. \tag{85}$$

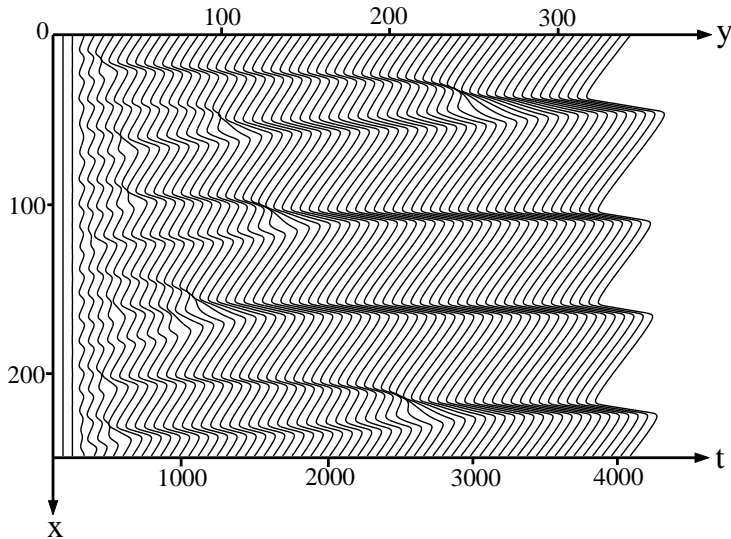


FIG. 6: Numerical simulation of Eq. (83). Time evolution of a single step for  $\rho = 0.001$  and  $\theta = 0.8$ . The step is systematically shifted in time (given by the lower axis). The electrical field is applied in the positive  $x$  direction.

Here  $H(x) = h_{-1}(x)$  and the time is rescaled such as  $\epsilon^4 t \rightarrow t$ . This amplitude equation is the central result of our study. As expected, this equation ensures mass conservation since its right hand side is a derivative of a mass current.

## V. NUMERICAL SIMULATIONS AND DISCUSSION

The time evolution of vicinal surfaces is obtained by integrating numerically Eq. (83). While the simulations are performed in the oblique frame  $(x, z)$ , the system is represented in the laboratory orthogonal frame  $(x, y)$ . Solving this stiff partial differential equation necessitates the use of an adaptive time step. A single step with periodic boundary conditions is simulated in practice. The whole vicinal surface is obtained by reproducing this step periodically along the  $\tilde{z}$  direction. The elastic interactions included in our model are not only justified from a purely physical point of view but are also a necessary ingredient in realistic numerical simulations. Indeed, test simulations performed without elastic interactions systematically resulted in step crossings at late times.

We first compare the dynamics of one step in two physical regimes defined by the values of the nondimensional number  $\rho = \frac{\nu L_0}{D_s}$ . For  $\rho > 1$ , the system dynamics is diffusion-limited,

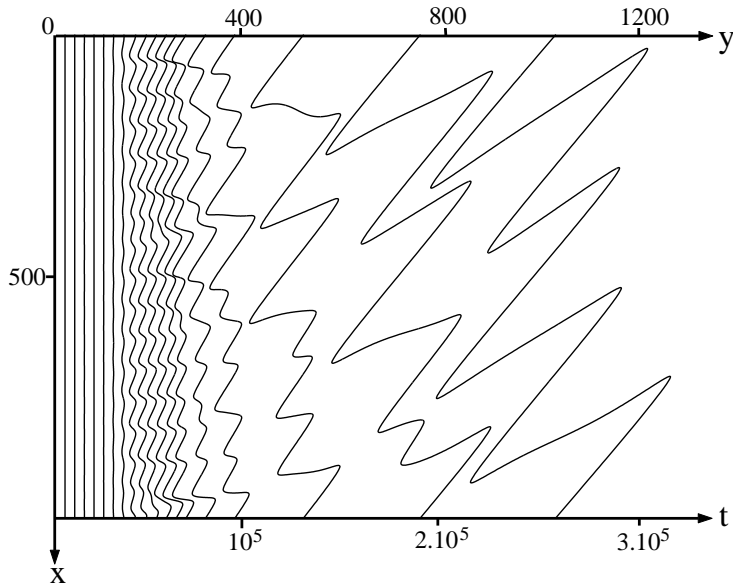


FIG. 7: Same as in Fig. (6) for  $\rho = 20$  and a larger system width.

while it is attachment-limited for  $\rho < 1$ . All the parameters ( $\alpha, \beta, \eta_2, \sigma$ ) entering Eq. (83) are set to unity here, and Figs. (6) and (7) show the time evolution of a single step for  $\rho = 0.001$  and  $\rho = 20$ , respectively. At short times, the steps are rather similar in shape for both values of  $\rho$ . Calculating the wave length emerging at short times, we find that it increases with  $\rho$  as predicted by the linear stability analysis. Alternatively, the growth rate  $\Gamma$  is found to decrease with  $\rho$ . At late times, after coarsening has set in, the step shapes differ strongly: a single-valued function is found in the laboratory frame for  $\rho = 0.001$ , while long overhangs are visible for  $\rho = 20$ . In both cases, the electrical field triggers local faceting of the steps which look like asymmetrical saw-teeth. Ultimately, the meander amplitude saturates to a finite value in a finite size system.

The time evolution of two vicinal surfaces is displayed in Figs.(8) and (9). Dark regions correspond to a high step density in which the electrical field is essentially oriented in the step-down direction, while it is mainly oriented in the step-up direction in the low step density regions. This result is consistent with the well-known step bunching observed for Si (111) when the heating current is applied perpendicular to the steps, in the step-down direction<sup>10</sup>.

According to the nature of the material, the surface orientation and the temperature range, physical parameters such as the diffusion coefficient may vary a lot. In addition,

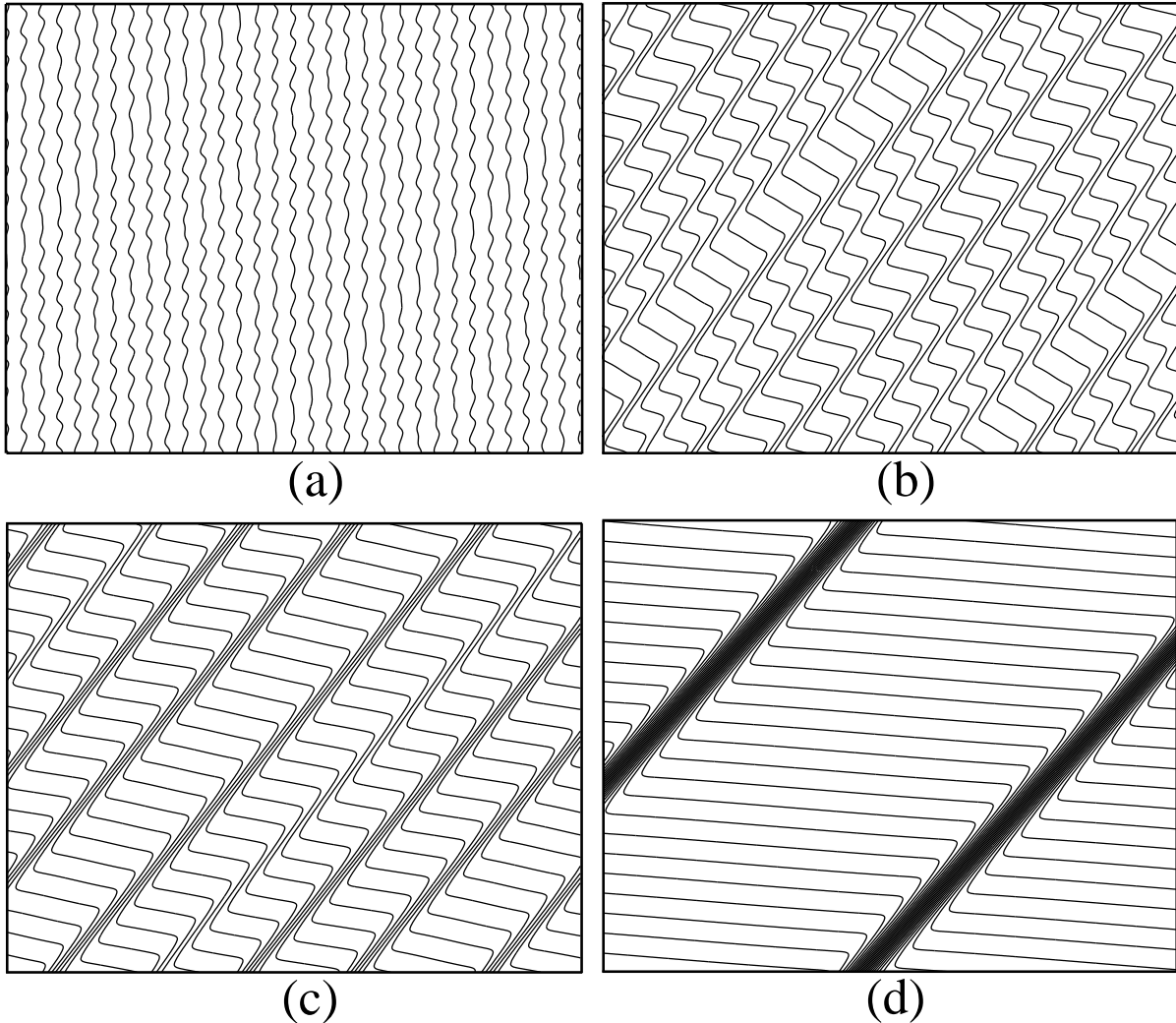


FIG. 8: Top view of a vicinal surface computed at different times for the same parameters as in Fig. (6): a)  $t = 230$ , b)  $t = 1200$ , c)  $t = 8300$ , d)  $t = 1.75 \times 10^5$ . The step down direction is righthwards while the electrical field direction is downwards.

they are not always known with a great accuracy. For example, for a Si(111) surface, four acceptable sets of physical parameters are given in table I of ref.<sup>12</sup>, of which set B seems particularly consistent with the experimental observations. For this particular set of physical parameters, Eq. (14) gives  $d = L_0/\rho = 5 \times 10^{-7}$ m. A miscut angle of one degree, then results in  $\rho \simeq 0.03$ , thus attachment/detachment-limited dynamics. Note that with the parameter sets A, C, or D, and/or a different miscut angle,  $\rho$  may vary in wide range, both below and above one. Our model is valid in both cases and it predicts rather different step shapes at long times, as just discussed. Experimental observation of vicinal surfaces under an electrical

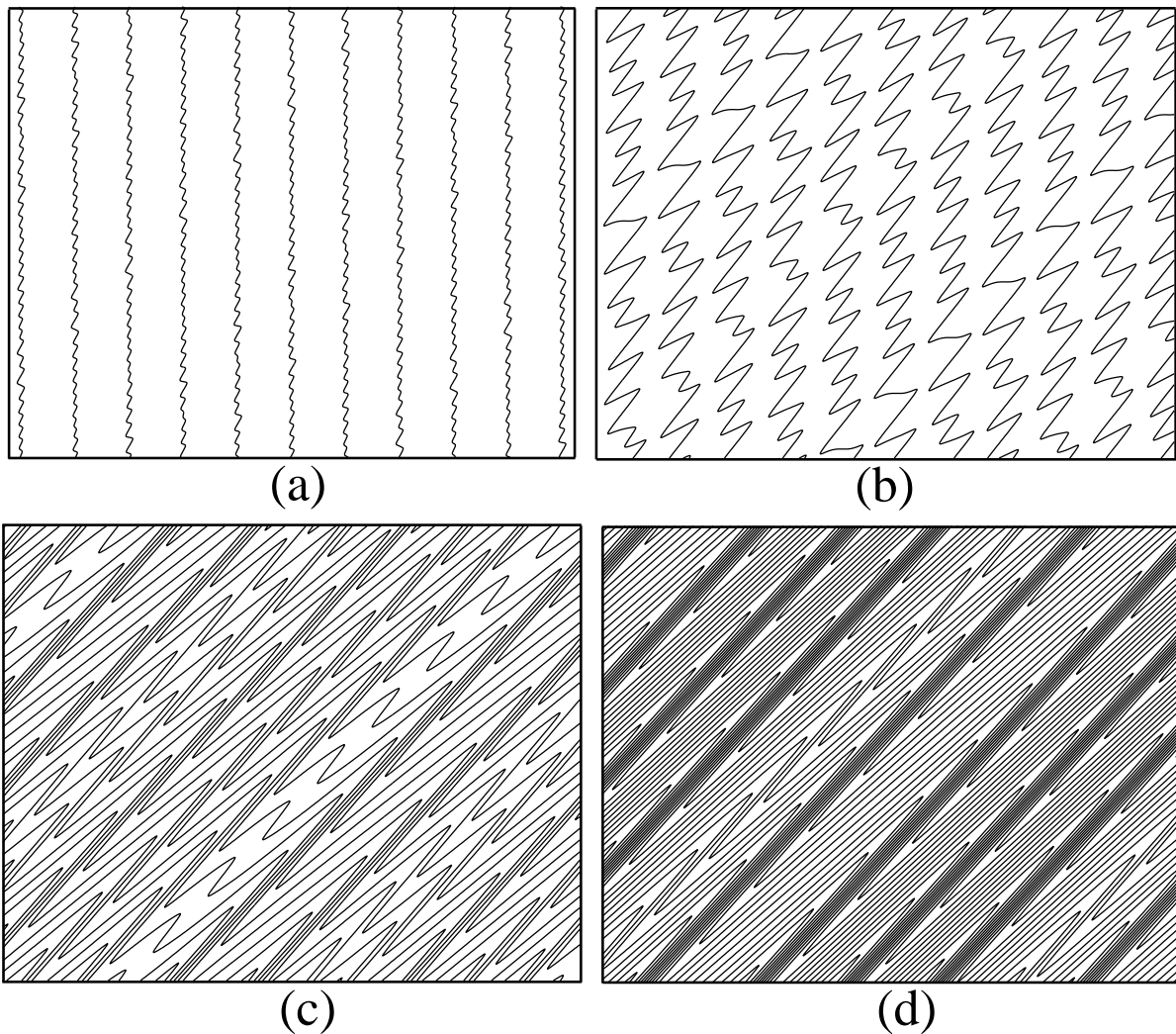


FIG. 9: Top view of a vicinal surface computed at different times for the same parameters as in Fig. (7): a)  $t = 6.4 \times 10^3$ , b)  $t = 1.6 \times 10^5$ , c)  $t = 8 \times 10^5$ , d)  $t = 3 \times 10^6$ . The step down direction is righthwards while the electrical field direction is downwards.

field parallel to the initial steps could possibly give an indication on the magnitude of the nondimensional number  $\rho$  which governs the system dynamics.

## VI. CONCLUSION AND PERSPECTIVES

In summary, we have studied the meandering instability induced by a constant electrical field initially parallel to a train of straight steps. The time evolution of the meanders is described by a nonlinear amplitude equation which we have derived through an asymptotic

expansion. Numerical simulations have been performed both in the attachment/detachment-limited ( $\rho \ll 1$ ) and the diffusion-limited ( $\rho \gg 1$ ) regimes. At large times, overhangs are observed in the latter case only.

It is very instructive to compare our results with an experimental study of step meandering on Si (111) vicinal surfaces, in which the orientation of the electrical field  $E$  is taken different from the step-down direction<sup>20</sup>. When  $E$  is set parallel to the steps, as in the present study, a similar step meandering effect is observed but the steps bend in the opposite direction as compared to our model. This apparent contradiction is in fact not unexpected because the experiments are performed at  $T = 1100^\circ\text{C}$ . Indeed, in this intermediate range of temperature ( $1000^\circ\text{C} - 1180^\circ\text{C}$ ), the steps have been argued to become transparent to the diffusing adatoms<sup>20</sup>. The underlying physics is thus expected to differ from the one introduced in our model (impermeable steps) and an opposite direction of bending is not contradictory. In the light of this discussion, new experiments performed at temperatures slightly higher than  $T = 1180^\circ\text{C}$  or slightly lower than  $T = 1000^\circ\text{C}$  would be desirable to test our model.

In the present model, consecutive steps are assumed identical up to a given phase-shift. Removing this phase constraint would allow a realistic description of experiments on a large scale. However, this can hardly be envisaged on the basis of the present method and a quite different point of view should be considered, such as a continuous limit approach. In addition, it would be helpful to include the step transparency in order to compare the resulting model to the experiments in the intermediate range of temperatures.

## Acknowledgments

It is a pleasure to acknowledge F. Leroy, J. J. Métois, C. Misbah, P. Müller, and A. Verga for fruitful discussions.

---

<sup>1</sup> A. Pimpinelli and J. Villain, *Physics of Crystal Growth* (Cambridge University Press, 1998).

<sup>2</sup> Y. Saito, *Statistical Physics of Crystal Growth* (World Scientific, 1998).

<sup>3</sup> H.-C. Jeong and E. D. Williams, *Surf. Sci. Rep.* **34**, 171 (1999).

<sup>4</sup> P. Politi, G. Grenet, A. Marty, A. Ponchet, and J. Villain, *Phys. Rep.* **324**, 271 (2000).

- <sup>5</sup> K. Yagi, H. Minoda, and M. Degawa, Surf. Sci. Rep. **43**, 45 (2001).
- <sup>6</sup> O. Pierre-Louis, Surf. Sci. **529**, 114 (2003).
- <sup>7</sup> J. Stangl, V. Holy, and G. Bauer, Rev. Mod. Phys. **76**, 725 (2004).
- <sup>8</sup> M. Schimschak and J. Krug, Phys. Rev. Lett. **78**, 278 (1997).
- <sup>9</sup> P. Kuhn, J. Krug, F. Hausser, and A. Voigt, Phys. Rev. Lett. **94**, 166105 (2005).
- <sup>10</sup> A. V. Latyshev, A. L. Aseev, A. B. Krasilnikov, and S. I. Stenin, Surf. Sci. **213**, 157 (1989).
- <sup>11</sup> S. Stoyanov, Jpn. J. Appl. Phys. **30**, 1 (1991).
- <sup>12</sup> D.-J. Liu. and J. D. Weeks, Phys. Rev. B **57**, 14891 (1998).
- <sup>13</sup> S. Stoyanov, Surf. Sci. **464**, L715 (2000).
- <sup>14</sup> J. J. Métois, J. C. Heyraud, and S. Stoyanov, Surf. Sci. **486**, 95 (2001).
- <sup>15</sup> W. K. Burton, N. Cabrera, and F. C. Frank, Philos. Trans. R. Soc. London, Ser. A **243**, 299 (1951).
- <sup>16</sup> A. Saúl, J.-J. Métois, and A. Ranguis, Phys. Rev. B **65**, 075409 (2002).
- <sup>17</sup> J. Krug, V. Tonchev, S. Stoyanov, and A. Pimpinelli, Phys. Rev. B **71**, 045412 (2005).
- <sup>18</sup> J. Chang, O. Pierre-Louis, and C. Misbah, Phys. Rev. Lett. **96**, 195901 (2006).
- <sup>19</sup> O. Pierre-Louis, Phys. Rev. Lett. **96**, 135901 (2006).
- <sup>20</sup> M. Degawa, H. Minoda, Y. Tanishiro, and K. Yagi, Phys. Rev. B **63**, 045309 (2001).
- <sup>21</sup> D.-J. Liu., J. D. Weeks, and D. Kandel, Phys. Rev. Lett. **81**, 2743 (1998).
- <sup>22</sup> G. S. Bales and A. Zangwill, Phys. Rev. B **41**, 5500 (1990).
- <sup>23</sup> A. Pimpinelli, I. Elkinani, A. Karma, C. Misbah, and J. Villain, J. Phys.: Condens. Matter **6**, 2661 (1994).
- <sup>24</sup> I. Bena, C. Misbah, and A. Valance, Phys. Rev. B. **47**, 7408 (1993).
- <sup>25</sup> O. Pierre-Louis, C. Misbah, Y. Saito, J. Krug, and P. Politi, Phys. Rev. Lett. **80**, 4221 (1998).
- <sup>26</sup> J. Kallunki and J. Krug, Phys. Rev. E **62**, 6229 (2000).
- <sup>27</sup> F. Gillet, O. Pierre-Louis, and C. Misbah, Eur. Phys. J. B **18**, 519 (2000).
- <sup>28</sup> S. Paulin, F. Gillet, O. Pierre-Louis, and C. Misbah, Phys. Rev. Lett. **86**, 5538 (2001).
- <sup>29</sup> G. Danker, O. Pierre-Louis, K. Kassner, and C. Misbah, Phys. Rev. Lett. **93**, 185504 (2004).
- <sup>30</sup> T. Frisch and A. Verga, Phys. Rev. Lett. **96**, 166104 (2006).
- <sup>31</sup> T. Frisch and A. Verga (2006), cond-mat/0607553, submitted to Physica D.
- <sup>32</sup> M. Sato, M. Uwaha, and Y. Saito, Phys. Rev. B **62**, 8452 (2000).
- <sup>33</sup> M. Sato, M. Uwaha, Y. Saito, and Y. Hirose, Phys. Rev. B **67**, 125408 (2003).



<sup>34</sup> M. Sato, M. Uwaha, and Y. Saito, *Phy. Rev. B* **72**, 045401 (2005).